

CFD MODELLING OF THE ACOUSTIC STREAMING INDUCED BY AN ULTRASONIC HORN REACTOR

Francisco Javier TRUJILLO¹ and Kai KNOERZER²

¹ CSIRO Food and Nutritional Sciences, North Ryde, New South Wales 2113, AUSTRALIA

² CSIRO Food and Nutritional Sciences, Werribee, Victoria 3030, AUSTRALIA

*Corresponding author, E-mail address: Francisco.Trujillo@csiro.au

ABSTRACT

Power ultrasonic reactors have gained a lot of interest in the food industry given the effects that can arise from sound induced cavitation. However, most of the new food processing developments have been based on empirical approaches. Thus, there is a need for mathematical models which help to understand, optimise and scale up ultrasonic reactors. In this work, a CFD model has been developed, to predict the acoustic streaming induced by an ultrasonic horn reactor. In the model it is assumed that the horn tip is a fluid inlet, where a turbulent jet flow is injected into the vessel. The hydrodynamic momentum rate of the incoming jet is assumed to be equal to the total acoustic momentum rate emitted by the acoustic power source. CFD predictions show excellent agreement with the experimental data at all studied power densities. This model successfully describes hydrodynamic fields (streaming) generated by ultrasound fields.

NOMENCLATURE

b	Characteristic width of the jet approach 1 (m)
c	Speed of sound (1480 m s ⁻¹)
\vec{F}	Force vector per unit of volume (N m ⁻³)
F_j	j component of \vec{F}
F_N	force or momentum rate (N)
\vec{I}	Sound intensity vector (W m ⁻²)
K	kinematic momentum (Kg m ⁻¹ s ⁻¹)
p	pressure (Pa)
P	Total acoustic power absorbed by the fluid (W)
r	radial distance (m)
r_H	horn radius (0.0065 m)
s	measure of the width of the jet approach 2 (m)
\vec{v}	velocity vector (m s ⁻¹)
v	velocity (m s ⁻¹)
x	distance from the orifice (m)
x	distance from acoustic source (m)
x_i	i component of position vector
β	attenuation or absorption coefficient (m ⁻¹)
C_μ	constant (0.09)
ε	Energy dissipation rate (m ² s ⁻³)
κ	turbulent kinetic energy (m ² s ⁻²)
t	length scale (m)
ρ	density (1000 kg m ⁻³)
μ	dynamic viscosity (Pa s)
μ_t	turbulent viscosity (Pa s)

INTRODUCTION

Ultrasound has found several new applications in the processing food industry over the last two decades (Mason, Paniwnyk et al. 1996). Power ultrasound can be used to enhance oxidation processes, such as aging of wines and spirits (Mason 1998); for bacteria inactivation in raw whole milk (Bermúdez-Aguirre, Corradini et al. 2009); to enhance the extraction of bioactives (Vilkhu, Mawson et al. 2008); and to improve solubility and foam properties of whey protein suspensions (Jambrak, Mason et al. 2008). These sonication technologies are based on the effects of cavitation, which is the formation of bubbles generated by pressure changes during the propagation of high intensity ultrasonic waves in liquids. The bubbles grow and then collapse during the compression passage of waves resulting in local temperatures of up to 5000 K and pressures of up to 50 MPa (Suslick 1988). These extreme conditions can generate sonoluminescence, hydroxyl radicals, streaming and enormous shear forces, which are responsible for the effects caused by sonication.

Most of the new food processing developments, however, have been based on time- and labour-intensive trial-and-error approaches. Furthermore, scaling up of ultrasound processes has shown to being difficult due to the lack of understanding the interactions between the sound field and the subsequently generated flow. Hence, developing and validating mathematical models, describing hydrodynamic fields (streaming) generated by the acoustic field are needed to understand and optimise the design of ultrasound processes.

Acoustic streaming is a term that describes the time-average flow circulation near a vibrating surface, or the steady flow induced during the passage of an acoustic wave. The former is called Rayleigh streaming and is attributed to the friction at a solid boundary that is vibrating and in contact with a fluid (Nyborg 1958). The latter is called “quartz wind” or simply “acoustic streaming” and was observed when ultrasound piezoelectric quartz came into use (Riley 1998). This streaming is generated by a source that projects a sound beam into a fluid as observed in ultrasonic horn reactors. The absorption of the energy of the sound wave by the fluid is responsible for the induced flow (Nyborg 1953; Tjotta 1999).

In this work, a CFD model has been developed to predict the acoustic streaming induced by an ultrasonic horn

reactor. The model is based on the acoustic streaming theory proposed by (Lighthill 1978), who established that at powers above 4×10^{-4} W the acoustic streaming takes the form of an inertially dominated turbulent jet. Lighthill is credited as the founder of aeroacoustics, which explains the generation of noise in jet engines (Lighthill 1952; Lighthill 1954), and proposed the analogy that not only a jet can generate sound, but also sound generates turbulent jets. The model assumes that the horn tip is an inlet where all the acoustic energy absorbed by the liquid is converted in turbulent motion, the jet. Using this assumption, the Navier-Stokes and $\kappa - \varepsilon$ turbulent equations were solved using COMSOL Multiphysics to determine the hydrodynamic field in the reactor; the results were compared with the experimental data obtained by (Kumar, Kumaresan et al. 2006) .

MODEL DESCRIPTION

Rayleigh, Nyborg and Westervelt (RNW) streaming theory

(Rayleigh 1896), (Nyborg 1953) and (Westervelt 1953) established that streaming can be calculated from the Navier-stokes equation, neglecting the convective acceleration term, also called the inertia term (left hand side of equation 1):

$$\rho(\vec{v} \cdot \nabla \vec{v}) = -\nabla p + \mu \nabla^2 \vec{v} + \vec{F} = 0 \quad (1)$$

Where the force that causes the streaming is the spatial variation of the Reynolds stress:

$$F_j = -\frac{\partial(\overline{\rho v_i v_j})}{\partial x_i} \quad (2)$$

For plane waves, this force is commonly obtained from the attenuation of the sound field (Tjøtta 1999):

$$\vec{F} = -\frac{1}{c} \nabla \vec{I} \quad (3)$$

Approximate solutions have been derived based on the RNW theory to calculate the acoustic streaming (Nowicki, Secomski et al. 1997; Nowicki, Kowalewski et al. 1998). However, (Lighthill 1978) showed that neglecting the inertia term of the Navier-Stokes equation is true only for very slow flows called "creeping motion" at very low Reynolds numbers ($Re < 1$) and low sources of power.

Stuart Streaming

This term was introduced by (Lighthill 1978) to describe acoustic streaming at higher Reynolds numbers, resulting from the application of a concentrated high power acoustic beam. In this case, the inertia term in equation 1 must be included as initially proposed by (Stuart 1963):

$$\rho(\vec{v} \cdot \nabla \vec{v}) = -\nabla p + \mu \nabla^2 \vec{v} + \vec{F} \quad (4)$$

Applying the same solution by (Squire 1951) for equation 4 in the case when a concentrated force $F = P/c$ is applied by an acoustic beam of power P , Lighthill demonstrated that the streaming motion becomes a jet. Lighthill assumed that the acoustic source releases its power as a narrow beam, where the net force (or rate of momentum) at a distance X along the sound beam is:

$$F_N = \frac{P}{c} (1 - e^{-\beta X}) \quad (5)$$

This equation represents the force that causes streaming (jet flow) after attenuation of the sound intensity, and is equal to the rate of momentum delivered at the source P/c minus the acoustic momentum flow remaining where the beam has been attenuated by a factor $e^{-\beta X}$. The equation below represents the kinematic momentum, which also increases with distance (x) along the beam as:

$$K = \rho_0 F_N = \rho \frac{P}{c} (1 - e^{-\beta X}) \quad (6)$$

If the attenuation coefficient is very high, the streaming motion generated by the acoustic beam is a circular turbulent jet, delivering momentum at a rate P/c . (Schlichting 1979) showed that the mean flow of a turbulent jet is similar to the laminar jet solution by taking a constant eddy viscosity equal to:

$$\mu_t = 0.016(K)^{1/2} \quad (7)$$

Where $K = \rho P/c$.

For low attenuation coefficients, the eddy viscosity increases along the beam as the kinematic momentum increases according to equation 6. In that case, equation 7 must be used in conjunction with equation 6 to describe the increase of turbulent viscosity along the sound beam.

(Lighthill 1978) assumed that the velocity profile of the acoustically generated jet flow follows a Gaussian distribution:

$$v = \left(\frac{2K}{\pi S^2} \right)^{1/2} e^{[-(r/S)^2]} \quad (8)$$

Where r is the distance from the beam axis and $S = S(X)$ is a measure of the width of the jet. Equation 8 can be justified if the intensity of the projected sound beam has also a Gaussian form. This equation also satisfies the conservation of momentum rate of the generated jet:

$$\rho \int_0^{\infty} v^2 2\pi r dr = F_N \quad (9)$$

Problem description and CFD modelling

The experimental data of (Kumar, Kumaresan et al. 2006) was used to validate the model. The ultrasonic reactor is a cylindrical vessel with a diameter of 0.135 m and a volume of 2000 ml with a horn tip submerged 0.02 m into the liquid. The diameter of the horn tip is 0.013m. Three levels of power density were studied, 15, 25 and 35 kWm^{-3} , which corresponds to a total power of 30, 50 and 70 W, respectively. The power was measured via the calorimetric method. Table 1 summarizes the power density (P/V), power (P) and kinematic momentum ($K = \rho P/c$) of the experimental data of (Kumar, Kumaresan et al. 2006).

Leve	P/V (kWm ⁻³)	P (W)	K (kg m ⁻¹ s ⁻¹)
1	15	30	20.27
2	25	50	33.78
3	35	70	47.30

Table 1: Experimental acoustic power and kinematic momentum as determined by (Kumar, Kumaresan et al. 2006)

As indicated earlier, the model assumes that the horn tip is an inlet where all acoustic energy is released as a turbulent jet flow. This assumption is valid for high attenuation coefficients where the acoustic energy is absorbed at a short distance from the horn tip. The side of the horn is assumed to be an outlet. Both assumptions, the existence of inlet and outlet, are expected to accurately represent the flow field below the horn tip for high power acoustic sources. The validity of this assumption is verified with the agreement between experimental and simulated axial velocity below the horn tip as shown in the results section. The 2D axis-symmetric representation of the Navier-Stokes equation (eq 4) is solved in COMSOL Multiphysics along with the $\kappa - \varepsilon$ turbulent model.

Figure 1 shows the boundary conditions of the CFD model. For the inlet boundary condition, the turbulent viscosity is assumed constant and is calculated with equation 7. Given that the $\kappa - \varepsilon$ turbulent model requires two boundary conditions, the turbulent length scale (l) was calculated as:

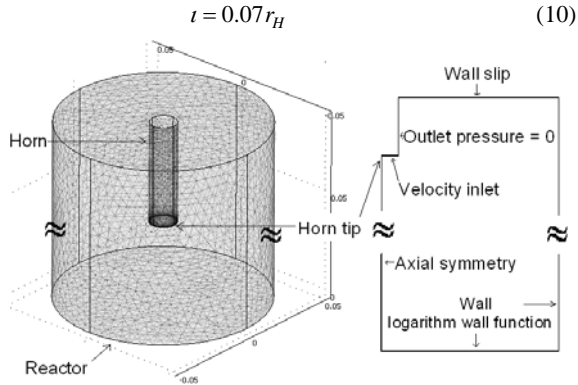


Figure 1: Schematic diagram of geometry (3D on the left) and boundary conditions (2D axial symmetric on the right).

With the turbulent viscosity and length scale:

$$\mu_t = \rho C_\mu \frac{\kappa^2}{\varepsilon} \quad (11)$$

$$l = \frac{\kappa^{3/2}}{\varepsilon} \quad (12)$$

κ and ε at the inlet are estimated as:

$$\kappa = \frac{\mu_t^2}{\rho^2 C_\mu^2 l^2} \quad (13)$$

$$\varepsilon = \frac{\kappa^{3/2}}{l} \quad (14)$$

The velocity profile at the inlet is calculated via the following two approaches:

Approach 1: Turbulent circular jet solution (Schlichting 1979)

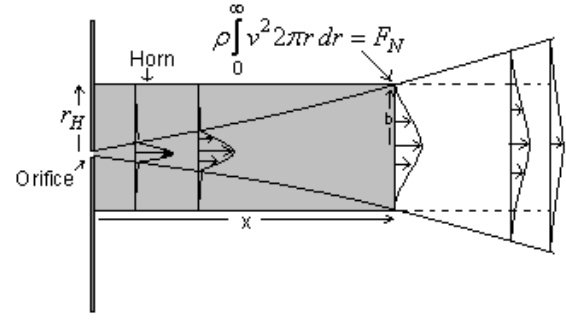


Figure 2: Schematic diagram of jet flow velocity profile superimposed in the horn.

Following this approach, the velocity profile at the inlet is estimated with equations taken from (Schlichting 1979) for a turbulent jet releasing its kinematic momentum from an orifice:

$$v = \frac{1}{4} \sqrt{\frac{3}{\pi}} \frac{\sqrt{K}}{x} \frac{\eta - \frac{1}{4}\eta^3}{\left(\eta + \frac{1}{4}\eta^2\right)^2} \quad (15)$$

$$\eta = \frac{1}{4} \sqrt{\frac{3}{\pi}} \frac{\sqrt{K} r}{\mu_t x} \quad (16)$$

Where x is the distance from the orifice. Figure 2 shows the velocity profile of such a jet flow, which must satisfy the conservation of momentum rate (c.f. eq. 9) at any distance x , and a superimposed horn. In the case of the acoustically generated jet flow the “orifice” is fictitious. Thus, x can be considered as a fitting parameter that modulates the velocity profile at the inlet releasing the same kinematic momentum (c. f. eq. 9). The figure also shows the characteristic width b of the jet, which changes linearly with x :

$$b = 2 \times 0.0848x \quad (17)$$

Therefore, it is expected that the radius of the horn r_H must be equal or greater than b to be able to release the kinematic momentum from the horn tip. That is the case for the three velocity profiles on the left hand side of figure 2 but not for the subsequent two profiles.

Approach 2: Gaussian jet velocity distribution (Lighthill 1978)

In this case the inlet velocity profile is calculated with equation 8, where the velocity is dependent on the kinematic momentum K , the radial distance r , and $S = S(X)$, which is a measure of the width of the streaming jet. Similarly to the previous approach, the conservation of momentum rate of the jet applies, and S can be considered as a fitting parameter to obtain a particular velocity profile.

RESULTS

Figure 3 shows a velocity distribution inside the ultrasonic reactor. This velocity pattern is in agreement with the experimental data obtained by (Kumar, Kumaresan et al. 2006) who mapped velocities and turbulence in the reactor using Laser Doppler Anemometry (LDA). They found that

ultrasonic horn reactors behave as if they were agitated with a downward plunging liquid jet, confirming the jet flow pattern induced at high power. Figure 4 shows the axial velocity below the horn tip for $P/V = 35 \text{ kWm}^{-3}$ using approach 1 for different distances to the fictitious jet “orifice”. The best fitting is obtained with $x = 0.025 \text{ m}$ by minimizing the root mean square error (RMSE). Figure 5 shows the inlet velocities obtained with x values from figure 4 using approach 1 and their equivalent velocity profiles based on approach 2. As seen in the figure both approaches can be used to obtain similar inlet velocity profiles. Interestingly x and S fit a straight line through the origin ($S = 0.1114x$), which reinforces the assumption of equivalence of both approaches to calculate the inlet velocity distribution.

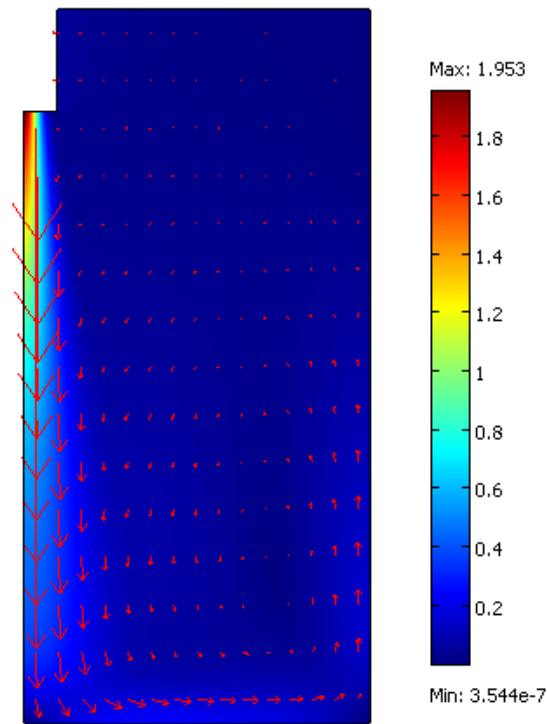


Figure 3: CFD velocity distribution predicted from approach 2 for $P/V = 35 \text{ kWm}^{-3}$ and $S = 0.00281$.

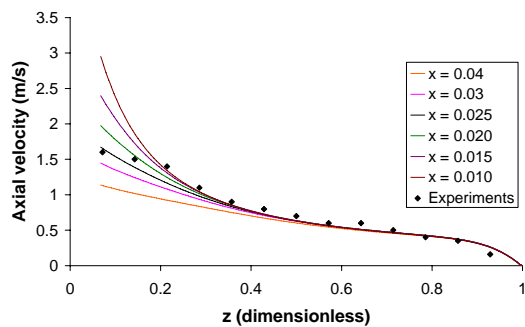


Figure 4: Axial velocity distribution below the horn tip using approach 1 for $P/V = 35 \text{ kWm}^{-3}$.

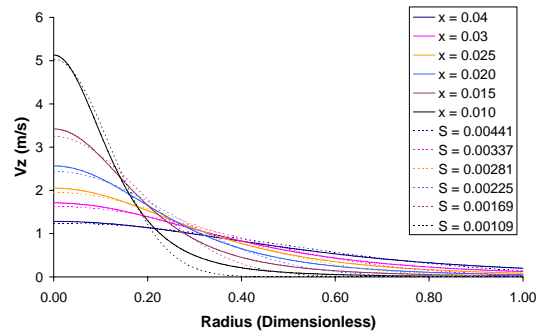


Figure 5: Inlet velocity profile for $P/V = 35 \text{ kWm}^{-3}$ at different x values using approach 1, and their corresponding s values using approach 2.

Optimum values of x and S for other power densities were also obtained by minimizing the RMSE. The final CFD prediction at three power densities can be seen in figure 6 using both approaches. CFD model predictions show an excellent agreement with the experimental data at all power densities. This confirms that x and S can be used as fitting parameter to adjust the velocity profile that releases the kinematic momentum to the fluid. The figure also shows that both approaches produce identical results; therefore they can be used interchangeably.

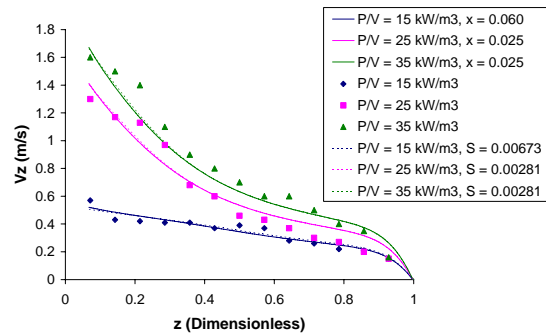


Figure 6: Axial velocity distribution below the horn tip using optimum values of x and S for approach 1 and 2 respectively.

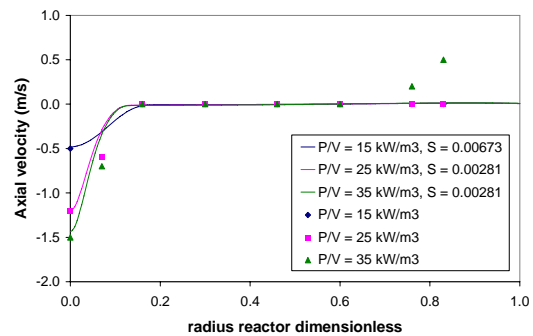


Figure 7: Radial profiles of axial velocity at different power densities for $z = 0.13H$. CFD prediction using approach 2 (solid lines)

Figure 7 shows the radial profiles of axial velocity at different power densities for $z = 0.13H$, where H is the distance between the horn tip and the bottom of the vessel. Again the CFD predictions show excellent agreement, except for regions close to the vessel wall at $P/V = 35 \text{ kWm}^{-3}$. Besides measuring the reactor flow

pattern, (Kumar, Kumaresan et al. 2006) also conducted CFD modelling using LDA measurements of axial, radial, tangential velocities and turbulence parameters (κ and ε) at four axial locations as input parameters, which were implemented in the CFD model as boundary conditions. Compared to their predictions, the model proposed in this study exhibits superior agreement with the measured data, and with the additional advantage of requiring only the acoustic power as input of the model and a fitting parameter (x or S).

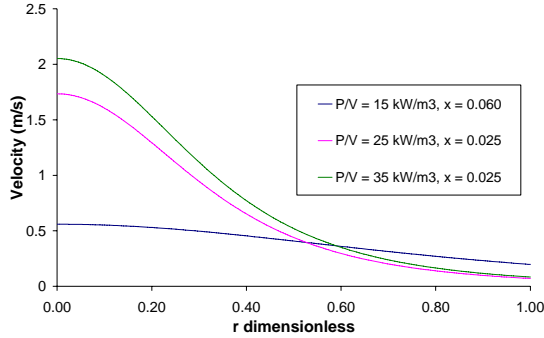


Figure 8: Inlet velocity profiles for optimum x values using approach 1 at different power densities

Figure 8 shows the velocity profiles at the inlet using approach 1 at optimum x values. Interestingly, optimum x values are equal to $x = 0.025$ for both: $P/V = 25$ and 35 kWm^{-3} , but has a different value ($x = 0.060$) for $P/V = 15 \text{ kWm}^{-3}$ (c.f. fig 8), suggesting a possible mechanism change between the lower and the two higher power densities. The same occurs when using approach 2 where $S = 0.0081$ for both: $P/V = 25$ and 35 kWm^{-3} , while $S = 0.00673$ for $P/V = 15 \text{ kWm}^{-3}$ (c.f. fig 6). This difference can be explained with table 2 where b , the characteristic width of the jet calculated via equation 16, is higher than the horn tip radius ($b = 11.024 \text{ mm}$, $r_H = 6.5 \text{ mm}$) for $P/V = 15 \text{ kWm}^{-3}$ but smaller than r_H for $P/V = 25$ and 35 kWm^{-3} . As explained in figure 2, r_H must be at least equal or greater than b to be able to release the totality of the kinematic momentum from the horn tip. Alongside the acoustic energy of the sound beam there is an acoustic momentum flow (Lighthill 1978); hence, the change of mechanism is likely that at lower power ($P/V = 15 \text{ kWm}^{-3}$) the acoustic rate of momentum cannot be fully absorbed and converted in hydrodynamic motion in the vicinity of the horn tip. The table also contains the total momentum rate $F = P/c$ calculated by equation 9 using both approaches, and the ratio:

$$\frac{P/c}{\rho \int_0^{r_H} v^2 2\pi r dr} \quad (18)$$

Which must be equal to 1 (100%) if all the acoustic rate of momentum is delivered at the inlet (for that reason the integral in equation 18 is evaluated between $r = 0$ and $r = r_H$). Both higher power densities, i.e. $P/V = 25$ and 35 kWm^{-3} , meet this criteria. Therefore, it can be concluded that for these high powers the assumption of high attenuation coefficient is valid and that the acoustic

energy is absorbed at a very short distance from the horn tip. Consequently, the totality of acoustic momentum rate is converted into hydrodynamic momentum rate in the vicinity of the source, further justifying the assumption of the horn tip as an inlet that releases all the kinematic momentum. This also helps to explain a finding reported by (Kumar, Kumaresan et al. 2006) that most of the turbulent kinetic energy (85%) is dissipated in the 2% of the volume near the horn tip.

For $P/V = 15 \text{ kWm}^{-3}$, the ratio from equation 18 is less than 100%, which means that the acoustic rate of momentum P/c is not completely absorbed and converted into fluid motion in close vicinity of the horn tip; the “effective” attenuation coefficient at this power should be smaller than for $P/V = 25$ and 35 kWm^{-3} . Consequently, sound beams irradiated from the source will be completely absorbed by the fluid and convert its acoustic energy into rate of momentum producing streaming over longer distances. In this case, equations 5 and 6 must be used incorporating the $e^{-\beta x}$ term. The difficulty in doing this is that the horn tip can not be simplified as an inlet, and modelling the system will require calculating the rate of momentum by tracking beams of sound from the source, where its intensity is attenuated while the kinematic momentum that causes streaming and the turbulent viscosity (c.f. eq. 7) increases along the beam. Tracking sound beams from the source to calculate the increase of rate of momentum and turbulent viscosity would be the correct procedure of modelling the system at $P/V = 15 \text{ kWm}^{-3}$ despite the excellent fit of the flow data, as a correct model should not only fit hydrodynamic profiles but also meet the law of momentum conservation as exhibited by $P/V = 25$ and 35 kWm^{-3} .

P/V	$F_N = P/c$ (N)	$F_N = \rho \int_0^{r_H} v^2 2\pi r dr$ (N)		$\frac{P/c}{\rho \int_0^{r_H} v^2 2\pi r ds}$ %		b (mm)
		App. 1	App. 2	App. 1	App. 2	
25	0.0338	0.0335	0.0338	99%	100%	4.24
35	0.0473	0.0469	0.0473	99%	100%	4.24

Table 2: Comparison rate of momentum calculated via equations 5 (after complete sound absorption) and 9.

“Effective” attenuation coefficients that allow total absorption of the acoustic energy in close vicinity of the source must have values several orders of magnitude higher than “molecular” attenuation coefficients reported in the literature (Piercy and Lamb 1954). This is expected, given that “molecular” attenuation coefficients are estimated via the RNW assumption, neglecting the inertia term as reported by (Piercy and Lamb 1954). Therefore, they will not represent attenuation at high acoustic power nor streaming induced with Reynolds numbers ($Re > 1$). Furthermore, “effective” attenuation coefficients account for the actual “observed” sound intensity attenuation, which can also be caused by scattering of sound waves by bubbles in a system exhibiting cavitation.

Although both approaches 1 and 2 produce very good results, approach 2 is preferred from a theoretical point of view, as it can be extended to cases of lower “effective” attenuation, where sound rays should be followed from the

source to calculate its intensity attenuation and subsequent increase of kinetic momentum (c.f. eq. 6) and turbulent viscosity (c.f. eq. 7), as explained by (Lighthill 1978). Approach 1 can be considered as supporting evidence which confirms the jet flow behaviour exhibited by high power acoustically induced streaming.

CONCLUSIONS

Acoustically induced ultrasound streaming at powers higher or equal than 30 W ($P/V \geq 15 \text{ kWm}^{-3}$) can be modelled via CFD by assuming that the horn tip is an inlet where a turbulent jet flow is injected into the vessel. The hydrodynamic rate of momentum of the incoming jet can be assumed to be equal to the total acoustic momentum rate P/c emitted by the acoustic power source.

CFD predictions show excellent agreement with the experimental data at all power densities via both approaches. Furthermore, the link between the acoustic and hydrodynamic field is straightforward: the only input needed to run the model is the absorbed acoustic power and a fitting parameter (x or S). Thus, this model successfully meets the objective of describing hydrodynamic fields (streaming) generated by the acoustic field.

There seems to be a change of mechanism between the lower and higher power densities (even though studied power levels are considered high power). For $P \geq 50 \text{ W}$ ($P/V \geq 25 \text{ kWm}^{-3}$) the assumption of high attenuation coefficients is valid and it can be concluded that the totality of acoustic momentum rate is converted into hydrodynamic momentum rate in close vicinity of the source, justifying the assumption that the horn tip is an inlet.

For $P < 50 \text{ W}$ ($P/V \leq 25 \text{ kWm}^{-3}$), sound beams irradiated from the source will take longer distances to complete absorption and to convert its acoustic energy into rate of momentum producing streaming. The model still shows an excellent agreement with the data, but does not meet the law of momentum conservation. Thus, despite the excellent agreement, the model should be modified by incorporating the $e^{-\beta x}$ term into equations 5 and 6.

REFERENCES

BERMÚDEZ-AGUIRRE, D., M. G. CORRADINI, et al. (2009). "Modeling the inactivation of *Listeria innocua* in raw whole milk treated under thermo-sonication." *Innovative Food Science & Emerging Technologies* **10**(2): 172-178.

JAMBRAK, A. R., T. J. MASON, et al. (2008). "Effect of ultrasound treatment on solubility and foaming properties of whey protein suspensions." *Journal of Food Engineering* **86**(2): 281-287.

KUMAR, A., T. KUMARESAN, et al. (2006). "Characterization of flow phenomena induced by ultrasonic horn." *Chemical Engineering Science* **61**: 7410-7420.

LIGHTHILL, J. (1952). "On Sound Generated Aerodynamically. I. General Theory " *Proceedings of the Royal Society of London. Series A, Mathematical and Physical* **211**(1107): 564-587.

LIGHTHILL, J. (1954). "On Sound Generated Aerodynamically. II. Turbulence as a Source of Sound " *Proceedings of the Royal Society of London. Series A, Mathematical and Physical* **222**(1148): 1954.

LIGHTHILL, J. (1978). "Acoustic streaming." *Journal of Sound and Vibration* **61**(3): 391-418.

MASON, T. J. (1998). *Power ultrasound in food processing - the way forward. Ultrasound in Food Processing*. M. J. W. Povey and T. J. Mason. London U. K., Blackie Academic & Professional: 105-126.

MASON, T. J., L. PANIWNKYK, et al. (1996). "The uses of ultrasound in food technology." *Ultrasonics Sonochemistry* **3**(3): S253-S260.

NOWICKI, A., T. KOWALEWSKI, et al. (1998). "Estimation of acoustical streaming: theoretical model, Doppler measurements and optical visualisation." *European Journal of Ultrasound* **7**(1): 73-81.

NOWICKI, A., W. SECOMSKI, et al. (1997). "Acoustic streaming: Comparison of low-amplitude linear model with streaming velocities measured by 32-MHz Doppler." *Ultrasound in Medicine & Biology* **23**(5): 783-791.

NYBORG, W. L. (1953). "Acoustic streaming due to attenuated plane waves." *The journal of the Acoustical Society of America* **25**(1): 68-75.

NYBORG, W. L. (1958). "Acoustic Streaming near a Boundary " *Journal of the Acoustical Society of America* **30**(4): 329-339.

PIERCY, J. E. and J. LAMB (1954). "Acoustic Streaming in Liquids " *Proceedings of the Royal Society of London. Series A, Mathematical and Physical* **226**: 43-50.

RAYLEIGH, L. (1896). *Theory of Sound*. New York, Dover Publications.

RILEY, N. (1998). "Acoustic streaming." *Theoretical and Computational Fluid Dynamics* **10**: 349-356.

SCHLICHTING, H. (1979). *Boundary Layer Theory*, McGraw-Hill.

SQUIRE, H. B. (1951). "The round laminar jet." *Quarterly Journal of Mechanical and Applied Mathematics* **4**: 321-329.

STUART, J. T. (1963). *Unsteady Boundary Layers. Laminar Boundary Layers*. L. Rosenhead. London, Oxford University Press.

SUSLICK, K. S. (1988). *Homogeneous Sonochemistry. Ultrasound, its Chemical, Physical and Biological effects*. K. S. Suslick. New York, VCH Publisher.

TJOTTA, S. (1999). "Theoretical Investigation of Heat and Streaming Generated by High Intensity Ultrasound." *Acustica* **85**: 780-787.

VILKHU, K., R. MAWSON, et al. (2008). "Applications and opportunities for ultrasound assisted extraction in the food industry -- A review." *Innovative Food Science & Emerging Technologies* **9**(2): 161-169.

WESTERVELT, P. J. (1953). "The Theory of Steady Rotational Flow Generated by a Sound Field " *Journal of the Acoustical Society of America* **25**: 68-75.